

Active Control of Irreversible Faradic Reactions to Enhance the Performance of Reverse Electrodialysis for Energy Production from Salinity Gradients

Oh, Yoontaek; Han, Ji Hyung; Kim, Hanki; Jeong, Namjo; Vermaas, David A.; Park, Jin Soo; Chae, Soryong

DOI

[10.1021/acs.est.1c02734](https://doi.org/10.1021/acs.est.1c02734)

Publication date

2021

Document Version

Accepted author manuscript

Published in

Environmental Science and Technology

Citation (APA)

Oh, Y., Han, J. H., Kim, H., Jeong, N., Vermaas, D. A., Park, J. S., & Chae, S. (2021). Active Control of Irreversible Faradic Reactions to Enhance the Performance of Reverse Electrodialysis for Energy Production from Salinity Gradients. *Environmental Science and Technology*, 55(16), 11388-11396. <https://doi.org/10.1021/acs.est.1c02734>

Important note

To cite this publication, please use the final published version (if applicable). Please check the document version above.

Copyright

Other than for strictly personal use, it is not permitted to download, forward or distribute the text or part of it, without the consent of the author(s) and/or copyright holder(s), unless the work is under an open content license such as Creative Commons.

Takedown policy

Please contact us and provide details if you believe this document breaches copyrights. We will remove access to the work immediately and investigate your claim.

1 **Active Control of Irreversible Faradaic Reactions to Enhance Performance of**
2 **Reverse Electrodialysis for Energy Production from Salinity Gradients**

3
4 Yoontaek Oh ¹, Ji-hyung Han ², Han-ki Kim ², Namjo Jeong ², David A. Vermaas ³, Jin-Soo Park
5 ^{4,*}, and Soryong Chae ^{1,*}

6
7 ¹ Department of Chemical and Environmental Engineering, University of Cincinnati, Cincinnati,
8 Ohio 45221, United States

9 ² Jeju Global Research Center, Korea Institute of Energy Research, Jeju-si, Jeju Province 63357,
10 Republic of Korea

11 ³ Department of Chemical Engineering, Faculty of Applied Sciences, Delft University of
12 Technology, 2629HZ, Delft, Netherlands

13 ⁴ Department of Green Chemical Engineering, College of Engineering, Sangmyung University, 31
14 Sangmyungdae-gil, Dongnam-gu, Cheonan-si, Chungnam Province 31066, Republic of Korea

15
16 * **Corresponding authors:** Dr. Jin-Soo Park (energy@smu.ac.kr) and Dr. Soryong Chae
17 (chaesg@ucmail.uc.edu)

18

19 **ABSTRACT**

20 Irreversible faradaic reactions in reverse electrodialysis (RED) are an emerging concern for scale-up,
21 reducing the overall performance of RED and producing environmentally harmful chemical species.
22 Capacitive RED (CRED) has the potential to generate electricity without the necessity of irreversible
23 faradaic reactions. However, there is a critical knowledge gap in the fundamental understanding of the
24 effects of operational stack voltages of CRED on irreversible faradaic reactions and the performance of
25 CRED. This study aims to develop an active control strategy to avoid irreversible faradaic reactions and
26 pH change in CRED, focusing on the effects of a stack voltage (0.9 – 5.0 V) on irreversible faradaic
27 reactions and power generation. Results show that increasing the initial output voltage of CRED by
28 increasing a stack voltage has an insignificant impact on irreversible faradaic reactions, regardless of the
29 stack voltage applied, but a cutoff output voltage of CRED is mainly responsible for controlling irreversible
30 faradaic reactions. The CRED system with eliminating irreversible faradaic reactions, achieved a maximum
31 power density (1.6 W m^{-2}) from synthetic seawater (0.513 M NaCl) and freshwater (0.004 M NaCl). This
32 work suggests that the control of irreversible faradaic reactions in CRED can provide stable power
33 generation using salinity gradients in large-scale operations.

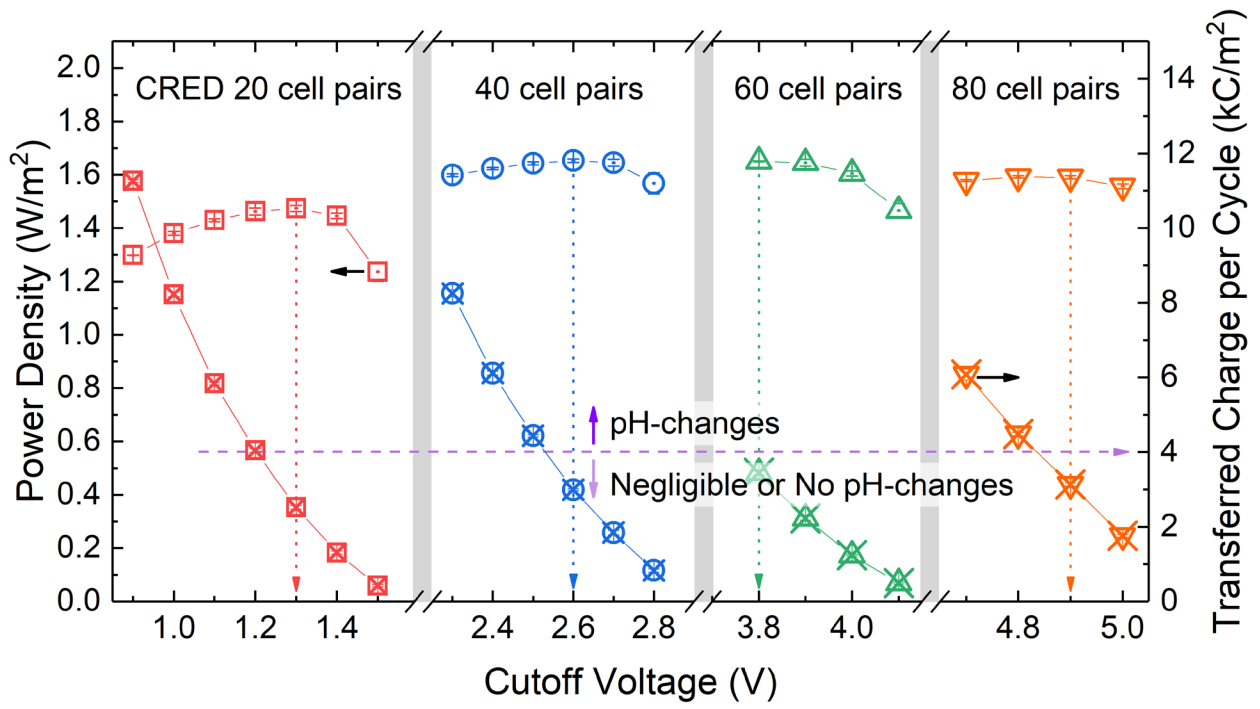
34

35 **Keywords:** capacitive reverse electrodialysis, irreversible faradaic reactions, pH change, salinity gradients,
36 power generation, stack voltage.

37

38 **Synopsis:** Capacitive reverse electrodialysis produces renewable energy from salinity gradients without
39 irreversible faradaic reactions, pH change, and environmentally harmful chemical species.

40 **Graphic for Table of Contents**



42 INTRODUCTION

43 When two aqueous solutions with different salinities are mixed through engineered systems, the salinity
44 gradient can create electric power. One of the most promising energy generation technologies that can
45 harvest electricity from salinity gradients is reverse electrodialysis (RED).¹⁻³ A RED stack with alternately
46 stacked cation exchange membranes (CEMs) and anion exchange membranes (AEMs) utilizes the chemical
47 potential of the salinity difference between two solutions to create an electrical potential over the membrane.
48 The stack of membrane pairs is sandwiched by a pair of electrodes, where the chemical potential is
49 converted into electricity *via* either reversible or irreversible faradaic reactions. Therefore, in addition to
50 the membrane pairs itself, the electrode systems play a crucial role in power generation with RED.⁴⁻⁷

51 Depending on which faradaic reactions are adopted, electrode systems can be categorized into two
52 groups. The electrode systems adopting irreversible faradaic reactions and electrolytes could generate toxic
53 gas (*e.g.*, Cl₂) and explosive gas (*e.g.*, H₂).⁸⁻¹⁰ The gas-evolution processes, mainly caused by water
54 electrolysis, consume significant energy, ultimately reducing RED's net power generation.^{4,11,12} Moreover,
55 diffusion of chloride ion (Cl⁻) towards the electrode rinse solution is inevitable, as shielding membranes are
56 never perfectly selective, implying the electrode rinse solution (ERS) needs to be purified frequently to
57 avoid chlorine evolution. The other electrode systems adopting reversible faradaic reactions utilize either
58 reactive electrodes (*e.g.*, Cu or Zn) or inert electrodes with homogeneous redox couples (*e.g.*, Fe^{2+/3+} or
59 Fe(CN)₆^{3-/4-}).^{1,4,5,7,9} One of the main advantages of these electrode systems is that the overall chemical
60 reaction is null, which consumes much lower energy than irreversible faradaic reactions during redox
61 reactions.

62 In RED, inert electrodes with homogeneous redox couples are more favorable than reactive electrodes
63 due to the better energy efficiency and the more straightforward design of the stack.^{4,5,7} However, they also
64 face operational limitations.¹³ For example, Fe(CN)₆^{3-/4-} can be decomposed into cyanide (a highly toxic
65 chemical compound) under sunlight and oxygen or acidic conditions (at accidental overcharging), and
66 Fe^{2+/3+} can form precipitations above pH 2 – 3.^{4,6,11,14} Moreover, some inert electrodes, for instance,

67 platinum-coated electrodes, are rather expensive but not proper for irreversible faradaic reactions in
68 electrode systems.⁴

69 Although a RED system adopts a redox couple, it can still generate harmful gases from irreversible
70 faradaic reactions when operated at a high stack voltage. Han et al. (2019) reported that gas evolution took
71 place continuously in the pilot-scale RED system with a pair of inert electrodes and $\text{Fe}(\text{CN})_6^{3-/4-}$ redox
72 couple due to water electrolysis.¹² This phenomenon took place because the concentration polarization of
73 the redox couple easily occurs locally in large stacks with high stack voltages, which leads to large (local)
74 overpotentials for the $\text{Fe}(\text{CN})_6^{3-/4-}$ redox couple, exceeding the minimum potential of water electrolysis (*i.e.*,
75 theoretically 1.23 V as standard electrode potential). Blue precipitation was also observed at the anode
76 where oxidation reactions took place, indicating that ferricyanide ($\text{Fe}(\text{CN})_6^{3-}$) was decomposed due to the
77 abrupt pH changes caused by water electrolysis.¹²

78 In contrast, Nam et al. (2019) deliberately employed water electrolysis for the RED system with 1,000
79 cell pairs to reduce costs and eliminate environmental impacts from using chemicals, such as redox couples.
80 ¹⁵ However, water electrolysis caused undesirable inorganic fouling by magnesium hydroxide and calcium
81 carbonate precipitates on the cathode due to the excessive presence of hydroxide ions (OH^-), leading to a
82 decrease in the RED performance. Therefore, it is paramount to adopt a proper electrode system for RED
83 that maintains the performance while mitigating the environmental impacts at the high stack voltage.

84 There is an alternative engineered system using cost-effective and sustainable electrode systems.
85 Capacitive mixing (CapMix) adopts capacitive electrodes. In CapMix, an externally applied electric
86 potential charges the electrodes immersed in a highly concentrated solution with opposite ions. When the
87 external potential is replaced with external load, and the high concentration solution is switched to a low
88 concentration solution, the accumulated ions are discharged from the electrodes, producing electrical
89 power.^{16,17} CapMix equipped with ion exchange membranes (IEMs) enables charging and discharging of
90 the electrodes without the external potential, which showed improved performance; however, the achieved
91 power density was limited at $0.007 - 0.2 \text{ W m}^{-2}$.^{18,19}

92 A new concept process has been developed to address the challenges associated with RED and CapMix
93 systems (*i.e.*, the environmental concerns and low power density). For example, Vermaas et al. (2013)²⁰
94 developed a capacitive RED (CRED) process by integrating RED and CapMix with activated carbon
95 capacitive electrodes but without the use of redox couples that showed 0.95 W m^{-2} at 3 – 4 V from synthetic
96 seawater (0.508 M NaCl), freshwater (0.017 M NaCl), and electrolyte (0.25 M NaCl).²⁰

97 The use of capacitive electrodes has been successfully demonstrated for several other electrochemical
98 membrane technologies, including desalination and energy generation technologies.^{13,21} However, the
99 performance of the capacitive electrode system has been constrained by relatively small-scale membrane
100 cell pairs at a low stack voltage than the previous study²⁰, which leads to a poor understanding of a scaled-
101 up capacitive electrode system at a high stack voltage that is much higher than that needed for water
102 electrolysis to occur. Since the current density and corresponding electrode overpotential determine the
103 range of practical operation for the CRED technology, the study of the performance behavior of the scaled-
104 up CRED can provide insight into the optimal operating conditions of the system and the potential for an
105 alternative RED configuration.

106 This study aims to develop an active control strategy of CRED to avoid irreversible faradaic reactions,
107 focusing on the effects of stack voltage of the CRED system on pH change and power generation in an
108 advanced CRED stack. While the voltage drop between the electrode and ERS determines irreversible
109 faradaic reactions, including water electrolysis, the stack voltage is adopted as a practical approach to
110 control irreversible faradaic reactions and pH.

111 The constant load (CL) discharge technique that facilitates continuous power generation is applied to
112 figure out the critical factors, such as cutoff voltages (*i.e.*, the voltage where the feed solutions are switched)
113 and the number of cell pairs, which influences the CRED performance. Finally, the maximum power density
114 obtained with different cell pairs in a bench-scale CRED is compared with a conventional RED.

115

116

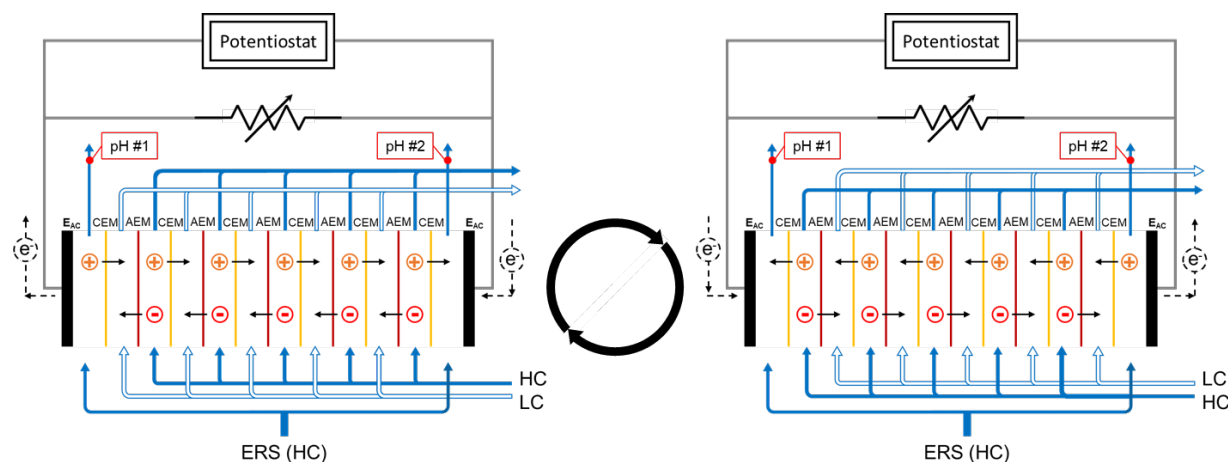
117 MATERIALS AND METHODS

118 **A Bench-scale CRED and RED.** Figure 1 shows a schematic diagram of a bench-scale CRED
119 system. The system is composed of AEMs, CEMs, polytetrafluoroethylene (PTFE) gaskets (0.1 mm
120 thickness) and spacers (0.1 mm thickness) between the membranes, and a pair of activated carbon (AC)
121 capacitive electrodes (Sion Tech Co., South Korea) at the end compartments. The AC loading of the
122 electrode is approximately 9 mg cm^{-2} . The projected area of the electrode was 19.6 cm^2 (5 cm in diameter).
123 All electrodes were immersed in 0.513 M NaCl (Fisher Scientific) solution under vacuum for 4 hours before
124 use in the CRED system. The CRED system with various cell pairs (20 – 80 cell pairs) of CEM (CEM-
125 Type I, FUJIFILM Manufacturing Europe B.V.) and AEM (AEM-Type I, FUJIFILM Manufacturing
126 Europe B.V.) was tested. The membranes were stored in 0.513 M NaCl solution at $4 \text{ }^\circ\text{C}$ before use. Each
127 cell pair has an effective area of 39.3 cm^2 .

128 Synthetic high concentration (HC) (0.513 M NaCl) and low concentration (LC) (0.004 M NaCl)
129 solutions were prepared by dissolving NaCl in deionized water ($1 - 2 \text{ } \mu\text{S cm}^{-1}$). The initial conductivity of
130 the HC and LC solutions were $48.5 \pm 0.1 \text{ mS cm}^{-1}$ and $500 \pm 5 \text{ } \mu\text{S cm}^{-1}$ at room temperature ($22 \pm 1 \text{ }^\circ\text{C}$),
131 respectively. Note that the conductivity of LC represents river water conductivity.²² The initial pH of the
132 HC and LC feed solutions were 6.0 ± 0.1 and 5.7 ± 0.1 , respectively. The same composition of HC solution
133 was also used as ERS.

134 Two feed solutions were fed into feed solution compartments at 5 mL min^{-1} per compartment using a
135 peristaltic pump (Cole-Parmer). The ERS was fed into the electrode compartments at 5 mL min^{-1} per
136 compartment using a peristaltic pump while the circuit was opened. It usually took less than one minute to
137 obtain a stable voltage of the system (data not shown). Once stabilized, an external resistor was connected,
138 and the system started discharging. When the voltage decreased below cutoff, the feed solutions were
139 switched, which completed a half-cycle. The experiments repeated at least four cycles (*i.e.*, eight half-cycles)
140 unless stated otherwise. Still, results are shown excluding the first cycle as the system showed a stable and
141 reliable voltage profile after the first cycle.

142 A conventional RED system is the same as the CRED system, except for the electrodes and the ERS.
 143 A bench-scale conventional RED system with platinum-coated titanium mesh electrodes (5 cm diameter,
 144 Wesco Electrode, South Korea) was tested in this study. A mixed solution that consists of 0.05 M potassium
 145 ferricyanide ($K_3[Fe(CN)_6]$), 0.05 M potassium ferrocyanide ($K_4[Fe(CN)_6]$), and 0.1 M sodium sulfate
 146 (Na_2SO_4) (Junsei Chemical Co.) was used as the ERS and fed into the system at 50 mL min^{-1} using a
 147 peristaltic pump. The conventional RED details can be found in our previous study.²³
 148



149
 150 **Figure 1.** Schematic diagram of a bench-scale CRED system and operating sequences. The system consists
 151 of multiple cell pairs (5 cell pairs in this diagram) and a pair of activated carbon electrodes (E_{AC}). Each cell
 152 pair consists of a CEM and an AEM. HC and LC solutions flow through the channels alternately and are
 153 switched periodically. The potentiostat measures the voltage of the system.

154
 155 **Characterization of AC Electrodes and Membranes.** Scanning electron microscope (SEM)
 156 coupled with energy-dispersive X-ray spectroscopy (EDX) (Scios DualBeam, Thermo fisher scientific)
 157 characterized surface morphology and structure of the AC electrode and membranes. Specific surface area,
 158 average pore diameter, and cumulative pore volume of the AC electrode were measured and calculated
 159 based on the Brunauer-Emmett-Teller (BET) method (ASAP 2060, Micromeritics) with nitrogen as the

160 analysis adsorptive at 77 K. The sample was dried overnight and degassed using nitrogen gas at 200 °C to
161 remove moisture in the sample.

162 The electrochemical characterization of the AC electrode was performed using a potentiostat (SP-150,
163 BioLogic) with a three-electrode system in 1 M KCl (Sigma-Aldrich) aqueous electrolyte. The working
164 electrode, the counter electrode, and the reference electrode were the AC electrode, platinum gauze (52
165 mesh, MilliporeSigma), and Ag/AgCl electrode (BioLogic), respectively. The cyclic voltammetry (CV)
166 curve was obtained at 5 mV s⁻¹ under the potential window of -0.5 V through +0.5 V. Galvanostatic
167 charge/discharge cycles were performed at 0.25, 0.5, and 1 A g⁻¹ under the same potential window.

168 **Assessment of CRED and RED Performance.** In this study, the CL discharge technique was
169 adopted to assess the CRED performance, eliminating an intermittent current interrupt time and
170 continuously producing energy. The CRED system was connected to the potentiostat that measured voltage
171 and an external resistor that produced energy in parallel. Using the resistance and its voltage, the average
172 power and the average power density can be calculated using the following equations^{20,24}

$$P = \frac{1}{t - t_0} \sum \frac{\Delta E^2}{R_{ext}} \times \Delta t \quad (1)$$

$$P_d = \frac{P}{N_{cell} A_{cell}} \quad (2)$$

173 where P is the average power from the CRED system-generated per cycle (W), t_0 and t are the time in the
174 beginning and the end of the cycle (second), ΔE is the voltage of the resistors, which is the same for the
175 CRED system, R_{ext} is the external resistance (Ω), Δt is the time interval of the voltage measurement during
176 the process, which was one second for the current study, P_d is the average power density per cycle (W m⁻²),
177 N_{cell} is the number of cell pairs (-), and A_{cell} is the effective membrane area of a single cell pair (m²).

178 Similarly, the average amount of transferred charge per unit projected electrode area through the
179 external resistance per cycle was calculated using the following equation.

$$Q_d = \frac{1}{A_{ele}} \frac{1}{t - t_0} \sum \Delta I \times \Delta t \quad (3)$$

180 where Q_d is the average transferred charge per unit projected electrode area through the external resistor
181 per cycle ($C\ m^{-2}$), A_{ele} is the projected electrode area of an electrode (m^2), and ΔI is the current flowing
182 through the resistors (A). The pH variation at the cathode and anode of the system was monitored by
183 measuring the solution pH of the ERS effluents from the cathode and anode, respectively.

184 The performance of the CRED system was compared to that of the conventional RED system with the
185 CL discharge technique. In addition, to verify the validity of the CL discharge technique, the RED
186 performance is evaluated and compared using two other electrochemical techniques: linear sweep
187 voltammetry (LSV) and constant current (CC) chronopotentiometry (Figure S2).

188

189 RESULTS AND DISCUSSION

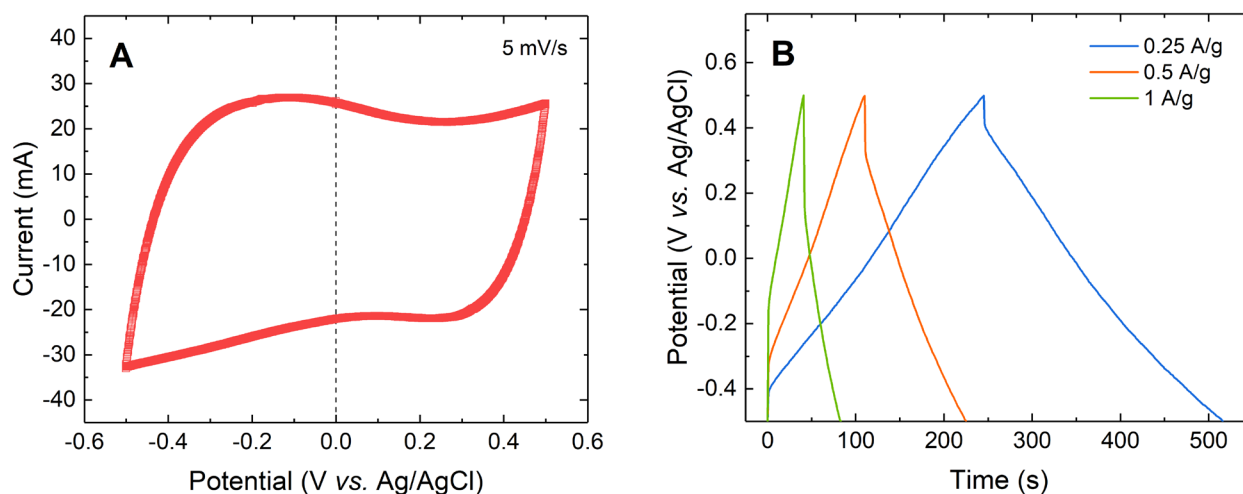
190 **Characteristics of AC Electrodes for CRED.** The AC electrode exhibited well-distributed fine
191 AC particles in contact with the graphite sheet current collector with an activated carbon layer thickness of
192 $150\ \mu m$ (Figure S3). The BET surface area and average pore size are $1173\ m^2\ g^{-1}$ and $2.1\ nm$, respectively
193 (Figure S4). The electrode is quite hydrophilic and good electrode material for the liquid electrolyte (Figure
194 S5).

195 The electrochemical properties of the AC electrode were evaluated using CV and galvanostatic
196 charge/discharge tests. Figure 2A shows the CV curve of the AC electrode at a fixed scan rate of $5\ mV\ s^{-1}$.
197 The AC electrode exhibits a quasi-rectangular CV profile without conspicuous gas evolution during the
198 measurement, demonstrating the typical behavior of an electric double-layer capacitor. Figure 2B shows
199 the galvanostatic charge/discharge curves of the AC electrode with various current densities ($0.25 - 1\ A\ g^{-1}$).
200 The specific capacitance was determined using the following equation.

$$C_s = \frac{I\Delta t}{\Delta V m} \quad (4)$$

201 where C_s is the specific capacitance ($F g^{-1}$), I is the discharge current (A), Δt is the discharge time (second),
202 ΔV is the potential change during discharge (V), and m is the weight of the AC loading on the electrode (g).
203 The symmetric charge/discharge characteristic for the AC electrode demonstrates the typical triangular
204 shape of ideal double-layer capacitor behavior. The specific capacitance of the AC electrode was $67.75 F$
205 g^{-1} ($= 0.610 F cm^{-2}$) at $0.25 A g^{-1}$, $57.5 F g^{-1}$ ($= 0.518 F cm^{-2}$) at $0.5 A g^{-1}$, $42 F g^{-1}$ ($= 0.378 F cm^{-2}$) at $1 A g^{-1}$,
206 respectively. At the beginning of the discharge curve at different discharge currents, the IR drop showed
207 the AC electrode internal resistance of 2.17Ω .

208



209 **Figure 2.** Electrochemical characterization showing CV curve at a scan rate of $5 mV s^{-1}$ (A) and
210 galvanostatic charge/discharge at different current densities ranging from 0.25 to $1 A g^{-1}$ (B) in $1 M KCl$
211 electrolyte solution.
212

213

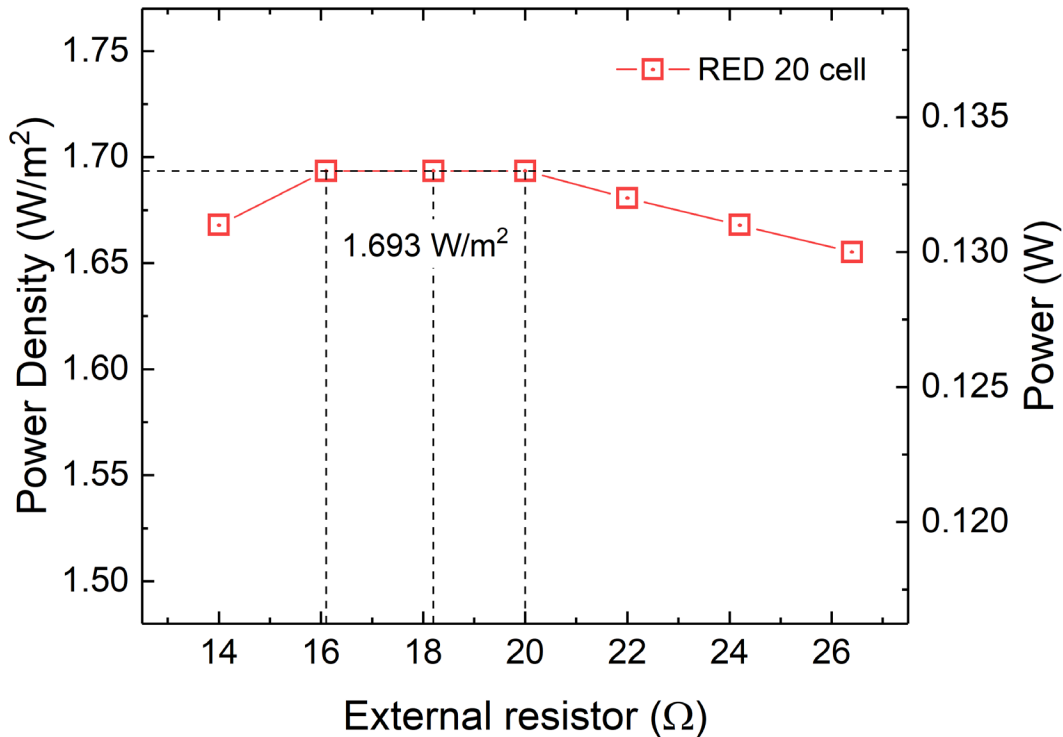
214 **Power Generation of RED.** The performance of a conventional RED system consisting of 20 cell
215 pairs was evaluated using the CL discharge technique (Figure 3). Various external resistors ($14 - 26.4 \Omega$)
216 with approximately 2Ω increments were tested to find an external resistance that gave the maximum power
217 density of the system. Each external resistor was connected to the RED system, and the voltage was logged.
218 The power density from the CL discharge technique was calculated using the following equation and Eq.
219 2.

$$P = \frac{\Delta E^2}{R_{ext}} \quad (5)$$

220 The maximum power density of 1.69 W m⁻² was obtained with the connected external resistors at 16.1,
 221 18.2, and 20 Ω, respectively. The operating voltage changed with connected external resistors (*i.e.*,
 222 increased with higher external resistances). Although it could be possible to obtain a little higher power
 223 density between 16.1 and 18.2 Ω or between 18.2 and 20 Ω, this would not differ significantly from the
 224 present result.

225 Based on the results, the external resistor of 18.2 Ω was selected as a representative external resistor
 226 that gave the maximum power density of the RED system with 20 cell pairs. The operating voltage was
 227 1.56 V when the 18.2 Ω resistor was connected to the RED system. The same procedure was applied to the
 228 RED system at different numbers of cell pairs (Table S1).

229



230

231 **Figure 3.** The power density of the conventional RED system consisting of 20 cell pairs obtained from
 232 constant load (CL) discharge with different external resistors.

233

234 **Effect of cutoff voltage on irreversible faradaic reactions and CRED performance.** Figure
235 4A shows voltage and power profiles of the CRED system consisting of 20 cell pairs connected to an
236 external resistor of 18.2 Ω at different cutoff voltages. The test was done between 0.9 – 1.5 V with a 0.1 V
237 difference, but only the selected data are shown. The different cutoff voltages resulted in the changes in
238 each cycle's maximum voltage, discharge time, and average power density. The lower cutoff voltage led to
239 a longer discharge time because the electrode discharged more ions, and therefore a larger fraction of the
240 available capacity was utilized.²⁴ Also, the cutoff voltage determined the maximum voltage in the following
241 half-cycle. The difference between the cutoff voltage and the maximum voltage in the following half-cycle
242 was found to be around 3.0 V for all cutoff voltages.

243 Therefore, ± 1.5 V was essentially the highest cutoff voltage, resulting in a symmetric voltage profile
244 for the current system setup. Moreover, the highest cutoff voltage was close to the operating voltage
245 obtained from the conventional RED system (1.56 V) under identical experimental conditions (20 cell pairs
246 connected to 18.2 Ω). Similarly, the highest cutoff voltage for the CRED system with 40, 60, and 80 cell
247 pairs was 2.8, 4.1, and 5.0 V, respectively, each of which is close to the operating voltages obtained from
248 the conventional RED system under identical experimental conditions (i.e., 2.85, 4.05, and 5.10 V,
249 respectively).

250 This relation originates from swapping the HC and LC fluids, which reverses the potential difference
251 over the RED membrane pairs. The total CRED stack voltage can be decomposed in a RED voltage (V_{RED}),
252 provided by the membrane pairs, and a capacitive potential at switching ($V_{C,switch}$) due to charge
253 accumulation at the electrodes. Upon switching, the HC and LC fluids, the V_{RED} switches to $-V_{RED}$, while
254 the sign of $V_{C,switch}$ remains the same. It can be described as switching at a cutoff voltage $V_{cutoff} = V_{RED} +$
255 $V_{C,switch}$ to opposite membrane potential, so $V_{max} = -V_{RED} + V_{C,switch}$, in which V_{max} is the highest
256 voltage obtained at the start of the new half-cycle in CRED (V). Combining these two equations yields the
257 highest cutoff voltage of the current CRED system for a symmetric voltage profile, as a function of the
258 operating voltage acquired from the conventional RED:

$$V_{cutoff} = 2V_{RED} + V_{max} \quad (6)$$

Please note that V_{max} always has an opposite sign compared to V_{cutoff} , $|V_{max}| \geq |V_{cutoff}|$, and V_{RED} which allows writing this as:

$$|V_{cutoff}| = 2V_{RED} - |V_{max}| \quad (7)$$

259 For the minimum cutoff voltage, side reactions need to be considered. The previous study by Vermaas
 260 et al. (2013)²⁰ reported that each half-cycle's voltage profile in the CRED process decreased linearly with a
 261 short switching interval (8 minutes). In contrast, the non-linear voltage profile was exhibited at the end of
 262 each half-cycle when a switching interval (*i.e.*, discharge time) was prolonged (33 minutes).²⁰ Note this
 263 previous study²⁰ adopted CC chronopotentiometry. The authors detected that the non-linear voltage profile
 264 and the pH changes appeared when the difference between the stack voltage (U_{CRED}) and the membrane
 265 voltage (U_{mem}) exceeds 0.9 V. U_{CRED} represents the overall CRED stack voltage that decreases with time
 266 because the system discharges. On the contrary, U_{mem} , representing the sum of the voltage over the
 267 membrane cells under given conditions, is constant because of the consistent salinity gradient maintained
 268 between two solutions and operating conditions in CRED.

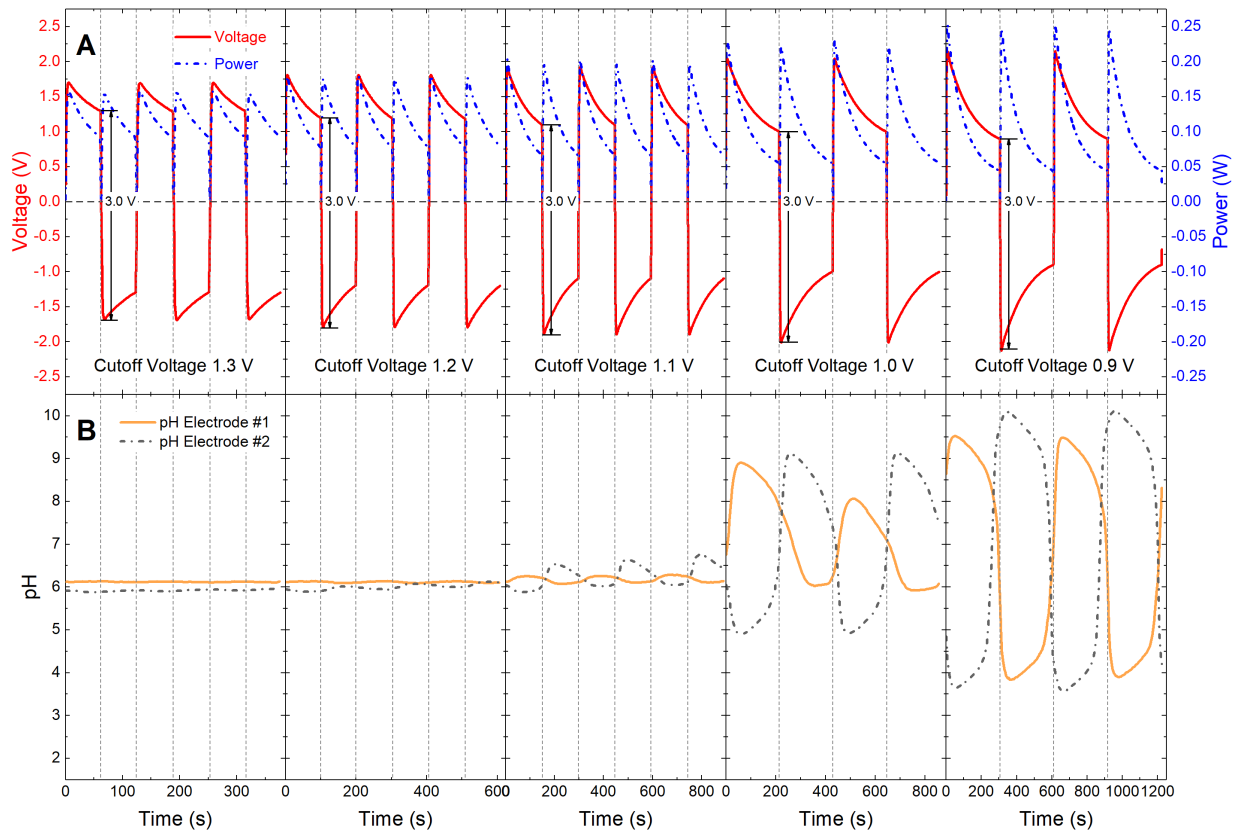
269 Similar but different trends were observed for the current CRED system with the CL discharge
 270 technique (Figure 4A and B). Since the lower cutoff voltage led to the larger amount of charge transferred,
 271 the lower cutoff voltage and, therefore, longer discharge time resulted in larger changes in pH. There are
 272 two distinct differences between the current study and the previous study.²⁰ First, in this study, the linearity
 273 of the voltage profile is inapplicable to determine whether the pH changes occur because when the
 274 capacitive electrode discharges through a constant resistor, the voltage drops exponentially. Second, the pH
 275 changes start from the cutoff voltage of 1.2 V (U_{CRED}), which is only about 0.36 V lower than the operating
 276 voltage 1.56 V (U_{mem}) from RED connected to 18.2 Ω and is much less than 0.9 V from the previous study.²⁰
 277 Moreover, as depicted in Figure 4C, when pH started fluctuating, approximately 4 kC m⁻² of the charge
 278 transferred. The fluctuation became exacerbated when lowering the cutoff voltages, which means that

279 irreversible faradaic reactions occurred on both electrode compartments. When the cutoff voltage was 0.9
280 V, approximately 11.2 kC m^{-2} of the charge transferred, the pH of effluent from the cathode increased to
281 10.1, and the pH of effluent from the anode decreased to 3.6.

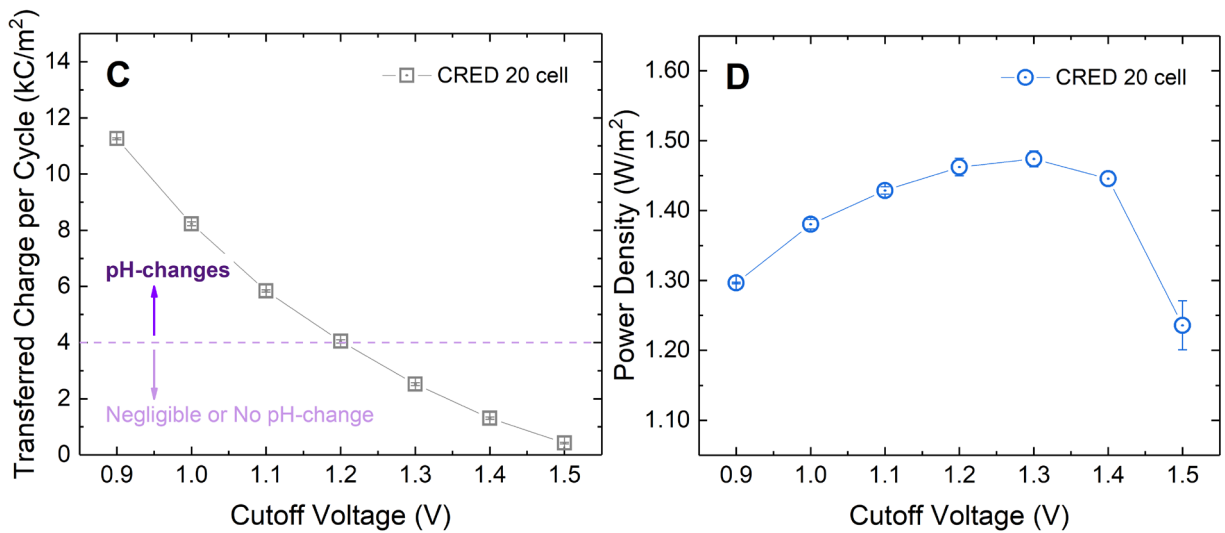
282 Recent studies on pH changes induced by high overvoltages in capacitive electrodes revealed that this
283 significant fluctuation in pH is attributed to irreversible faradaic reactions, including water oxidation and
284 reduction that generate H^+ and OH^- , respectively, and conceivably other irreversible faradaic reactions, such
285 as hydrogen peroxide (H_2O_2) generation and subsequent consumption that contribute to the pH changes in
286 capacitive electrochemical systems.²⁵⁻²⁹ However, it is complicated to distinguish which reactions are more
287 favorable than the others during the operation.

288 In addition, it was assumed that given the high concentration (0.513 M of NaCl) of ERS and the range
289 of the pH changes (i.e., pH 3.5 – 10), the AC electrode performance was not influenced by the pH changes
290 capacitance (mobility ratio H^+/Na^+ is about 6.9 and OH^-/Cl^- is about 2.6).²⁷ Isolating the effect of pH on
291 electrode performance would require a completely different study, which is complex and beyond the scope
292 of this study. Despite the complexity, it is obvious that the CRED power performance decreases with the
293 occurring pH changes.

294



295



296

297 **Figure 4.** The voltage and corresponding power profile (A) and the pH changes of the bench-scale CRED
 298 system with 20 cell pairs connected to an external resistor (18.2 Ω) between 0.9 – 1.5 V cutoff voltages (B),
 299 transferred charge per cycle (C), and the power densities at different cutoff voltages (D).

300

301 Figure 4D shows the overall power density of the CRED system with 20 cell pairs at the different cutoff
302 voltages. The power densities were increased from the cutoff voltages 1.5 to 1.3 V then started decreasing,
303 most likely due to irreversible faradaic reactions that consume energy generated from the salinity gradient.
304 Despite the earlier onset of pH changes in the electrode compartments, the power density is much higher
305 than for previous CRED work²⁰, thanks to optimized RED cells (lower resistances, higher salinity gradient)
306 and fast switching (which allows reducing the OCV interval between the switching). The detailed power
307 profiles and the average power densities are shown in Figure S6. The cutoff voltage of 1.5 V shows the
308 extreme of switching very frequently, which yields a lower power density than when using a cutoff voltage
309 of 1.3 V, revealing an inherent limitation of the CRED system; the necessity of a periodic switching of the
310 feed solutions to regenerate the electrodes.

311 The switching of feed solutions reverses the voltage polarity and the current direction, resulting in the
312 sudden drop in power generation during the switching period. For example, one full cycle at 1.5 V cutoff
313 voltage takes only approximately 24 seconds, including the switching period of approximately 8 – 9 seconds
314 (Figure S6A). More than 30% of the time per cycle for switching causes a decrease in average power and
315 power density.

316 On the other hand, the cutoff voltage of 0.9 V with a much longer discharge time and much higher peak
317 power than the other cutoff voltages also show a lower power density than 1.3 V (Figure S6D). The
318 prolonged discharge time due to irreversible faradaic reactions decreased the overall average power and the
319 power density. It is noteworthy that although the slight pH changes do not considerably decrease the
320 performance of the system (*e.g.*, the power density at 1.1 V cutoff voltage), the performance decline starts
321 with the pH changes in the electrode system.

322 Therefore, it is paramount to set cutoff voltage as low as possible unless the pH changes occur to obtain
323 a maximum power density. Together with the practical need for an indicator of the system to maximize
324 power generation, this result demonstrates that the CRED process can generate sustainable and comparable
325 power without significant pH changes.

326

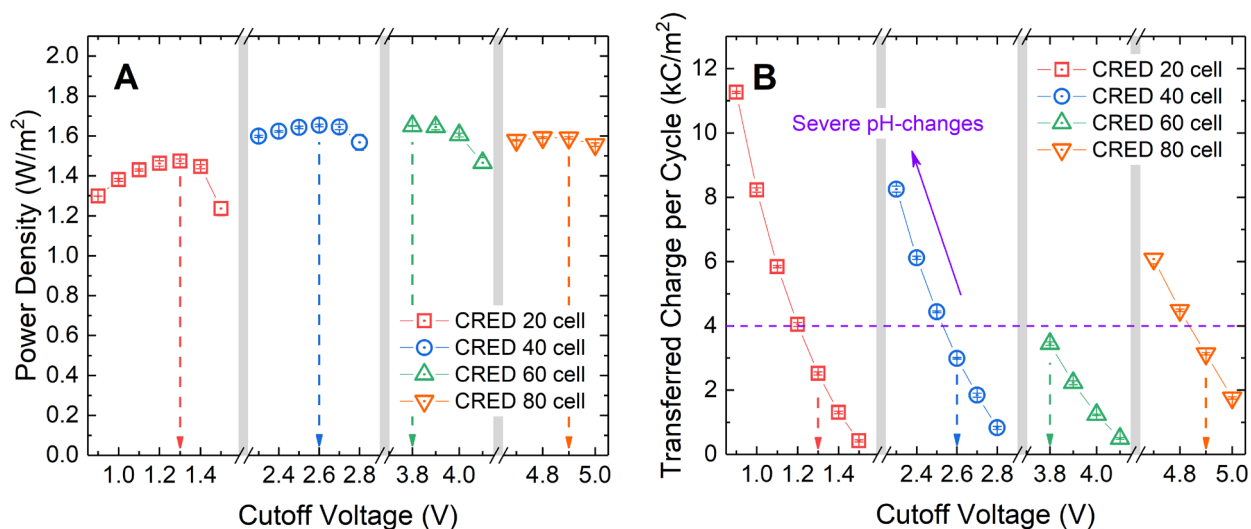
327 **Effect of Number of Cell Pairs.** The CRED system with 40, 60, and 80 cell pairs was connected to
328 external resistors of 30.1, 41.8, and 51.9 Ω , respectively. The maximum power densities of 40, 60, and 80
329 cell pairs are $1.65 \pm 0.01 \text{ W m}^{-2}$ at 2.6 V, $1.65 \pm 0.00 \text{ W m}^{-2}$ at 3.8 V, and $1.59 \pm 0.01 \text{ W m}^{-2}$ at 4.9 V cutoff
330 voltage, respectively (Figure 5A). Apparently, the maximum power density is obtained at the lowest cutoff
331 voltage without the pH changes, which is a similar trend of 20 cell pairs. The voltage differences between
332 the operating voltage (U_{mem}) and the cutoff voltage (U_{CRED}) where the pH changes start are 0.35, 0.35, and
333 0.3 V, respectively, which is consistent with the result of 20 cell pairs. For 80 cell pairs, the power density
334 at the cutoff voltage of 4.8 V ($1.59 \pm 0.00 \text{ W m}^{-2}$) is marginally higher than 4.9 V, but this accompanies the
335 pH changes. It is obvious that the lower the cutoff voltage applies, the more significant pH changes occur,
336 which leads to a decrease in the power density.

337 As shown in Figure 5B, the pH changes for all cell pairs correlate with the amount of charge transferred
338 strongly during discharge (Figure 5B). In this study, the pH changes started with the amount of transferred
339 charge over approximately 4 kC m^{-2} regardless of the number of cell pairs, which is much lower than the
340 reported value (*i.e.*, 20 kC m^{-2}) from Vermaas et al. (2013).²⁰ The difference is most likely due to the specific
341 capacitance or total capacitance of an electrode. The previous study²⁰ used the high-performance capacitive
342 electrode showing the specific capacitance of 1.2 F cm^{-2} (or total electrode capacitance of 120 F). In contrast,
343 the current study used the electrode that showed only 0.52 F cm^{-2} (or total electrode capacitance of 10 F).
344 Note that all discharge currents of CRED for maximum power density are in a range of approximately 80
345 – 100 mA, which is close to the current density of 0.5 A g^{-1} (88.4 mA) in galvanostatic charge/discharge.

346 A higher areal-specific capacitance means that a larger quantity of charge can be stored in the same
347 projected electrode area. Thus, it appears that a relatively sufficient charge in the same area is more capable
348 of prohibiting irreversible faradaic reactions. Consequently, the voltage where the pH changes occur may
349 vary and rather depends on the electrode characteristics, such as the specific capacitance or total capacitance.

350 Therefore, from the consistent results of the voltage difference and the amount of transferred charge, it
351 can be concluded that the pH changes in CRED depend on the electrode properties. Moreover, a longer
352 discharge time per cycle could be achieved by increasing the specific capacitance of electrodes since a

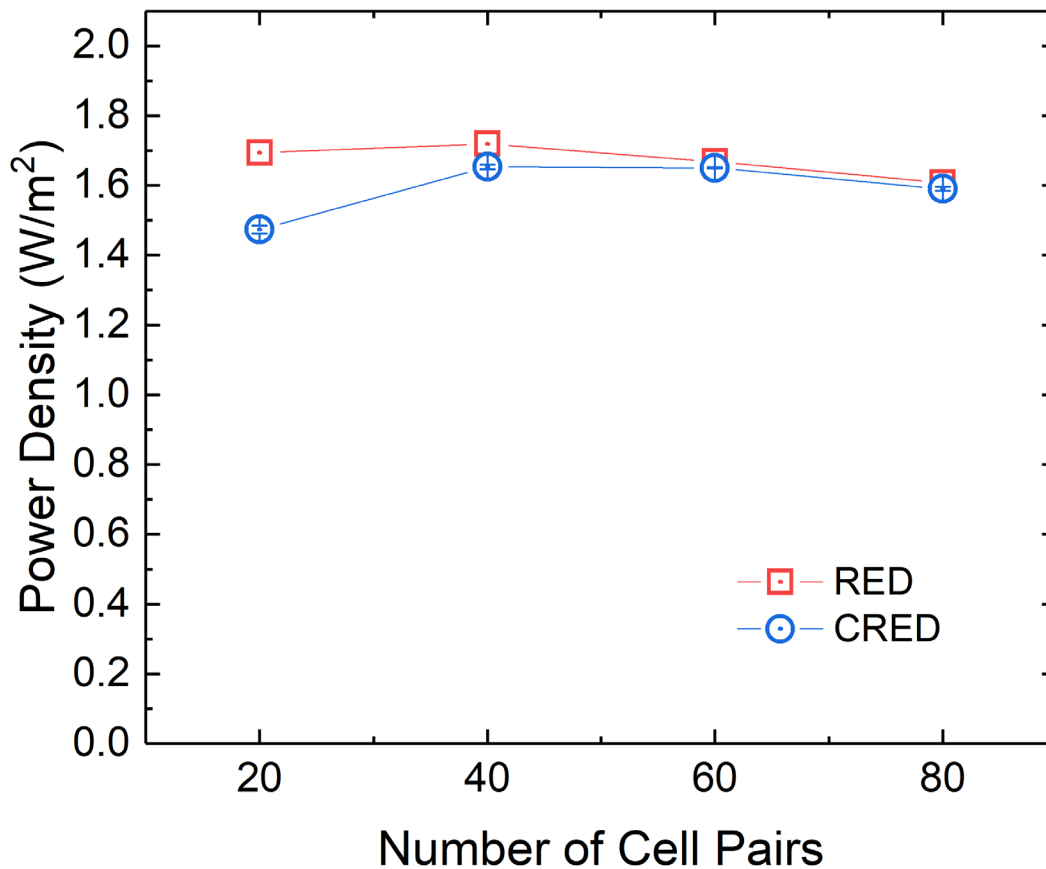
353 higher capacitance takes longer to discharge under identical conditions. The average time per cycle for 20,
 354 40, 60, and 80 cell pairs when the maximum power density is obtained is 125, 127, 141, and 126 seconds,
 355 respectively; this means approximately every minute, feed solutions need to be switched. It could be an
 356 issue in the context of the cost for frequent solution switching. In other words, extending the discharge time
 357 while maintaining the performance should be considered in actual facility-scale operations.
 358



359
 360 **Figure 5.** The power density of CRED at different cutoff voltages with different numbers of cell pairs. 18.2,
 361 30.1, 41.8, and 51.9 Ω were connected to the CRED system with 20, 40, 60, and 80 cell pairs, respectively
 362 (A). The amount of transferred charge and the pH changes at different cutoff voltages for all cell pairs (B).
 363 The dashed arrow indicates the cutoff voltage where the maximum power density is obtained. The dashed
 364 line indicates the amount of transferred charge per cycle where the pH changes starts.

365
 366 **CRED Performance vs. RED Performance.** Figure 6 shows the maximum power density of the
 367 bench-scale CRED and RED systems. The lower power density at 20 cell pairs is likely due to the electrical
 368 resistance of the electrode system. Considering the electrical resistance of the electrode system is constant,
 369 the power consumption by the electrode system may constrain the overall power density with a small
 370 number of cell pairs. When increasing the number of cell pairs, this power consumption becomes

371 insignificant. The maximum power densities obtained from CRED are only 1% lower than those from the
372 conventional RED for 60 and 80 cell pairs. Not only were the maximum power densities obtained at very
373 high operating voltages, but they were also obtained without irreversible faradaic reactions. The maximum
374 power density of approximately 1.6 W m^{-2} is much higher than any reported CapMix processes (*i.e.*, 0.007
375 $- 0.2 \text{ W m}^{-2}$)^{17-19,30,31} and even almost doubled compared to CRED in the previous study (*i.e.*, 0.95 W m^{-2}).²⁰
376
377



378
379 **Figure 6.** Comparison of the maximum power density of the bench-scale CRED and RED systems with
380 different numbers of cell pairs.

381
382 It is instructive to note that the main driving force for both RED and CRED systems is the Donnan
383 potential that is generated by salinity gradients across IEMs. However, the Ohmic resistance of the CRED

384 electrode pair weighs against the charge transfer resistance (*i.e.*, overpotential according to the Butler-
385 Volmer eq.) of quasi-reversible redox couples. In this study, the Ohmic resistance of the CRED electrode
386 pair is still higher; therefore, for the efficient conversion from the chemical potential to power, engineered
387 electrodes are needed.

388 Recent studies^{24,32} demonstrated that the electrode potential could be combined with the Donnan
389 potential in a concentration flow cell, resulting in improved power density. In those studies, a single IEM
390 and a pair of redox (average power density = 3.8 W m^{-2})²⁴ or capacitive electrodes (average power density
391 = 0.95 W m^{-2})³² was used to maximize the potentials from synthetic seawater (0.513 M NaCl) and
392 freshwater (0.017 M NaCl). However, when stacking IEMs between the electrodes, which is a typical RED
393 configuration, the influence of the electrode potential would be diminished as the number of cell pairs
394 increases. Thereby, the Donnan potential predominates the overall voltage and power density of the
395 concentration flow cell, which means the performance would not be different from a conventional RED.

396 Although a CRED stack cannot easily surpass the power density of a conventional RED stack with a
397 reversible redox couple, the main gain for capacitive electrodes is to be achieved in the elimination of
398 potentially irreversible or dangerous faradaic reactions. A large-scale RED suffers from undesired results,
399 including fouling and performance decline by irreversible faradaic reactions at a high stack voltage, as
400 evidenced by the previous studies.^{12,15} The current study shows that the CRED system can potentially
401 sustain and stabilize power generation without pH changes, even at high operating voltages.

402

403 **ASSOCIATED CONTENT**

404 The Supporting Information is available free of charge at xxxx.

405 **Supporting information**

406 A bench-scale CRED system (**Figure S1**), the power density of the conventional RED system co obtained
407 from linear sweep voltammetry (LSV), constant current, chronopotentiometry, constant load discharge, and

408 the maximum power density (D) (**Figure S2**), SEM images of the AC electrode (**Figure S3**), adsorption
409 and desorption isotherms of the AC electrode (**Figure S4**), the water contact angle on the AC electrode
410 surfaces with time (**Figure S5**), the detailed power profile of the CRED system with 20 cell pairs connected
411 to an external resistor (**Figure S6**), external resistance and corresponding operating voltage result in the
412 maximum power density of the conventional RED system at different numbers of cell pairs (**Table S1**).

413

414 **AUTHOR INFORMATION**

415 **Corresponding Authors**

416 **Jin-Soo Park** – Department of Green Chemical Engineering, College of Engineering, Sangmyung
417 University, 31 Sangmyungdae-gil, Dongnam-gu, Cheonan-si, Chungnam Province 31066, Republic of
418 Korea; orcid.org/0000-0003-4487-946X; Email: energy@smu.ac.kr

419 **Soryong Chae** – Department of Chemical and Environmental Engineering, University of Cincinnati,
420 Cincinnati, Ohio 45221, United States; orcid.org/0000-0002-2382-4075; Email: chaesg@ucmail.uc.edu

421

422 **Authors**

423 **Yoontaek Oh** – Department of Chemical and Environmental Engineering, University of Cincinnati,
424 Cincinnati, Ohio 45221, United States; orcid.org/0000-0002-7413-1033

425 **Ji-hyung Han** – Jeju Global Research Center, Korea Institute of Energy Research, Jeju-si, Jeju Province
426 63357, Republic of Korea; orcid.org/0000-0001-7577-392X

427 **Han-ki Kim** – Jeju Global Research Center, Korea Institute of Energy Research, Jeju-si, Jeju Province
428 63357, Republic of Korea; /orcid.org/0000-0002-0184-7356

429 **Namjo Jeong** – Jeju Global Research Center, Korea Institute of Energy Research, Jeju-si, Jeju Province
430 63357, Republic of Korea

431 **David A. Vermaas** – Department of Chemical Engineering, Faculty of Applied Sciences, Delft
432 University of Technology, Netherlands; orcid.org/0000-0002-4705-6453

433 **Notes** The authors declare no competing financial interest.

434

435 **ACKNOWLEDGMENTS**

436 This work was conducted under the framework of the Research and Development Program of the Korea
437 Institute of Energy Research (KIER) (Project Number: B8-2441).

438

439 **REFERENCES**

440 (1) Pattle, R. E. Production of Electric Power by Mixing Fresh and Salt Water in the Hydroelectric
441 Pile. *Nature* **1954**, *174*, 660. <https://doi.org/10.1038/174660a0>.

442 (2) Post, J. W.; Veerman, J.; Hamelers, H. V. M.; Euverink, G. J. W.; Metz, S. J.; Nymeijer, K.;
443 Buisman, C. J. N. Salinity-Gradient Power: Evaluation of Pressure-Retarded Osmosis and Reverse
444 Electrodialysis. *J. Memb. Sci.* **2007**, *288* (1–2), 218–230.

445 <https://doi.org/10.1016/j.memsci.2006.11.018>.

446 (3) Post, J. W.; Hamelers, H. V. M.; Buisman, C. J. N. Energy Recovery from Controlled Mixing Salt
447 and Fresh Water with a Reverse Electrodialysis System. *Environ. Sci. Technol.* **2008**, *42* (15),
448 5785–5790. <https://doi.org/10.1021/es8004317>.

449 (4) Veerman, J.; Saakes, M.; Metz, S. J.; Harmsen, G. J. Reverse Electrodialysis: Evaluation of
450 Suitable Electrode Systems. *J. Appl. Electrochem.* **2010**, *40* (8), 1461–1474.

451 <https://doi.org/10.1007/s10800-010-0124-8>.

452 (5) Scialdone, O.; Guarisco, C.; Grispo, S.; Angelo, A. D.; Galia, A. Investigation of Electrode
453 Material - Redox Couple Systems for Reverse Electrodialysis Processes. Part I: Iron Redox
454 Couples. *J. Electroanal. Chem.* **2012**, *681*, 66–75. <https://doi.org/10.1016/j.jelechem.2012.05.017>.

455 (6) Scialdone, O.; Albanese, A.; D'Angelo, A.; Galia, A.; Guarisco, C. Investigation of Electrode
456 Material - Redox Couple Systems for Reverse Electrodialysis Processes. Part II: Experiments in a
457 Stack with 10-50 Cell Pairs. *J. Electroanal. Chem.* **2013**, *704*, 1–9.

- 458 <https://doi.org/10.1016/j.jelechem.2013.06.001>.
- 459 (7) Lee, S. Y.; Jeong, Y. J.; Chae, S. R.; Yeon, K. H.; Lee, Y.; Kim, C. S.; Jeong, N. J.; Park, J. S.
460 Porous Carbon-Coated Graphite Electrodes for Energy Production from Salinity Gradient Using
461 Reverse Electrodialysis. *J. Phys. Chem. Solids* **2016**, *91*, 34–40.
462 <https://doi.org/10.1016/j.jpics.2015.12.006>.
- 463 (8) Weinstein, J. N.; Leitz, F. B. Electric Power from Differences in Salinity: The Dialytic Battery.
464 *Science* **1976**, *191* (4227), 557–559. <https://doi.org/10.1126/science.191.4227.557>.
- 465 (9) Jagur-Grodzinski, J.; Kramer, R. Novel Process for Direct Conversion of Free Energy of Mixing
466 into Electric Power. *Ind. Eng. Chem. Process Des. Dev.* **1986**, *25* (2), 443–449.
467 <https://doi.org/10.1021/i200033a016>.
- 468 (10) Turek, M.; Bandura, B. Renewable Energy by Reverse Electrodialysis. *Desalination* **2007**, *205* (1–
469 3), 67–74. <https://doi.org/10.1016/j.desal.2006.04.041>.
- 470 (11) D'Angelo, A.; Tedesco, M.; Cipollina, A.; Galia, A.; Micale, G.; Scialdone, O. Reverse
471 Electrodialysis Performed at Pilot Plant Scale: Evaluation of Redox Processes and Simultaneous
472 Generation of Electric Energy and Treatment of Wastewater. *Water Res.* **2017**, *125*, 123–131.
473 <https://doi.org/10.1016/j.watres.2017.08.008>.
- 474 (12) Han, J. H.; Hwang, K. sik; Jeong, H.; Byeon, S. Y.; Nam, J. Y.; Kim, C. S.; Kim, H.; Yang, S. C.;
475 Choi, J. Y.; Jeong, N. Electrode System for Large-Scale Reverse Electrodialysis: Water
476 Electrolysis, Bubble Resistance, and Inorganic Scaling. *J. Appl. Electrochem.* **2019**, *49* (5), 517–
477 528. <https://doi.org/10.1007/s10800-019-01303-4>.
- 478 (13) Liu, F.; Coronell, O.; Call, D. F. Electricity Generation Using Continuously Recirculated Flow
479 Electrodes in Reverse Electrodialysis. *J. Power Sources* **2017**, *355*, 206–210.
480 <https://doi.org/10.1016/j.jpowsour.2017.04.061>.
- 481 (14) Tedesco, M.; Scalici, C.; Vaccari, D.; Cipollina, A.; Tamburini, A.; Micale, G. Performance of the
482 First Reverse Electrodialysis Pilot Plant for Power Production from Saline Waters and
483 Concentrated Brines. *J. Memb. Sci.* **2016**, *500*, 33–45.

- 484 <https://doi.org/10.1016/j.memsci.2015.10.057>.
- 485 (15) Nam, J. Y.; Hwang, K. S.; Kim, H. C.; Jeong, H.; Kim, H.; Jwa, E.; Yang, S. C.; Choi, J.; Kim, C.
486 S.; Han, J. H.; Jeong, N. Assessing the Behavior of the Feed-Water Constituents of a Pilot-Scale
487 1000-Cell-Pair Reverse Electrodialysis with Seawater and Municipal Wastewater Effluent. *Water*
488 *Res.* **2019**, *148*, 261–271. <https://doi.org/10.1016/j.watres.2018.10.054>.
- 489 (16) Brogioli, D. Extracting Renewable Energy from a Salinity Difference Using a Capacitor. *Phys.*
490 *Rev. Lett.* **2009**, *103* (5), 058501. <https://doi.org/10.1103/PhysRevLett.103.058501>.
- 491 (17) Brogioli, D.; Zhao, R.; Biesheuvel, P. M. A Prototype Cell for Extracting Energy from a Water
492 Salinity Difference by Means of Double Layer Expansion in Nanoporous Carbon Electrodes.
493 *Energy Environ. Sci.* **2011**, *4* (3), 772–777. <https://doi.org/10.1039/c0ee00524j>.
- 494 (18) Sales, B. B.; Saakes, M.; Post, J. W.; Buisman, C. J. N.; Biesheuvel, P. M.; Hamelers, H. V. M.
495 Direct Power Production from a Water Salinity Difference in a Membrane-Modified
496 Supercapacitor Flow Cell. *Environ. Sci. Technol.* **2010**, *44* (14), 5661–5665.
497 <https://doi.org/10.1021/es100852a>.
- 498 (19) Liu, F.; Schaetzle, O.; Sales, B. B.; Saakes, M.; Buisman, C. J. N.; Hamelers, H. V. M. Effect of
499 Additional Charging and Current Density on the Performance of Capacitive Energy Extraction
500 Based on Donnan Potential. *Energy Environ. Sci.* **2012**, *5* (9), 8642–8650.
501 <https://doi.org/10.1039/c2ee21548a>.
- 502 (20) Vermaas, D. A.; Bajracharya, S.; Sales, B. B.; Saakes, M.; Hamelers, B.; Nijmeijer, K. Clean
503 Energy Generation Using Capacitive Electrodes in Reverse Electrodialysis. *Energy Environ. Sci.*
504 **2013**, *6* (2), 643–651. <https://doi.org/10.1039/c2ee23562e>.
- 505 (21) Campione, A.; Cipollina, A.; Toet, E.; Gurreri, L.; Bogle, I. D. L.; Micale, G. Water Desalination
506 by Capacitive Electrodialysis: Experiments and Modelling. *Desalination* **2020**, *473*, 114150.
507 <https://doi.org/10.1016/j.desal.2019.114150>.
- 508 (22) USGS Current Conditions for USGS 07374000 Mississippi River at Baton Rouge, LA
509 https://waterdata.usgs.gov/usa/nwis/uv?site_no=07374000.

- 510 (23) Oh, Y.; Jeong, Y.; Han, S. J.; Kim, C. S.; Kim, H.; Han, J. H.; Hwang, K. S.; Jeong, N.; Park, J.
511 S.; Chae, S. Effects of Divalent Cations on Electrical Membrane Resistance in Reverse
512 Electrodialysis for Salinity Power Generation. *Ind. Eng. Chem. Res.* **2018**, *57* (46), 15803–15810.
513 <https://doi.org/10.1021/acs.iecr.8b03513>.
- 514 (24) Kim, T.; Logan, B. E.; Gorski, C. A. High Power Densities Created from Salinity Differences by
515 Combining Electrode and Donnan Potentials in a Concentration Flow Cell. *Energy Environ. Sci.*
516 **2017**, *10* (4), 1003–1012. <https://doi.org/10.1039/c7ee00188f>.
- 517 (25) Kim, T.; Yu, J.; Kim, C.; Yoon, J. Hydrogen Peroxide Generation in Flow-Mode Capacitive
518 Deionization. *J. Electroanal. Chem.* **2016**, *776*, 101–104.
519 <https://doi.org/10.1016/j.jelechem.2016.07.001>.
- 520 (26) He, D.; Wong, C. E.; Tang, W.; Kovalsky, P.; David Waite, T. Faradaic Reactions in Water
521 Desalination by Batch-Mode Capacitive Deionization. *Environ. Sci. Technol. Lett.* **2016**, *3* (5),
522 222–226. <https://doi.org/10.1021/acs.estlett.6b00124>.
- 523 (27) Dykstra, J. E.; Keesman, K. J.; Biesheuvel, P. M.; van der Wal, A. Theory of PH Changes in
524 Water Desalination by Capacitive Deionization. *Water Res.* **2017**, *119*, 178–186.
525 <https://doi.org/10.1016/j.watres.2017.04.039>.
- 526 (28) Zhang, C.; He, D.; Ma, J.; Tang, W.; Waite, T. D. Faradaic Reactions in Capacitive Deionization
527 (CDI) - Problems and Possibilities: A Review. *Water Res.* **2018**, *128*, 314–330.
528 <https://doi.org/10.1016/j.watres.2017.10.024>.
- 529 (29) Liu, F.; Coronell, O.; Call, D. F. Effect of Cross-Chamber Flow Electrode Recirculation on PH
530 and Faradaic Reactions in Capacitive Deionization. *Desalination* **2020**, *492*, 114600.
531 <https://doi.org/10.1016/j.desal.2020.114600>.
- 532 (30) La Mantia, F.; Pasta, M.; Deshazer, H. D.; Logan, B. E.; Cui, Y. Batteries for Efficient Energy
533 Extraction from a Water Salinity Difference. *Nano Lett.* **2011**, *11* (4), 1810–1813.
534 <https://doi.org/10.1021/nl200500s>.
- 535 (31) Ye, M.; Pasta, M.; Xie, X.; Dubrawski, K. L.; Xu, J.; Liu, C.; Cui, Y.; Criddle, C. S. Charge-Free

536 Mixing Entropy Battery Enabled by Low-Cost Electrode Materials. *ACS Omega* **2019**, *4* (7),
537 11785–11790. <https://doi.org/10.1021/acsomega.9b00863>.
538 (32) Zhu, H.; Xu, W.; Tan, G.; Whiddon, E.; Wang, Y.; Arges, C. G.; Zhu, X. Carbonized Peat Moss
539 Electrodes for Efficient Salinity Gradient Energy Recovery in a Capacitive Concentration Flow
540 Cell. *Electrochim. Acta* **2019**, *294*, 240–248. <https://doi.org/10.1016/j.electacta.2018.10.053>.
541